

Instability of liquid Cu films on a SiO substrate

Alejandro Guillermo González, Javier Alberto Diez, Yueying Wu, Jason D. Fowlkes, Philip D. Rack, and Lou Kondic

Langmuir, **Just Accepted Manuscript** • DOI: 10.1021/la4009784 • Publication Date (Web): 27 Jun 2013

Downloaded from <http://pubs.acs.org> on July 1, 2013

Just Accepted

“Just Accepted” manuscripts have been peer-reviewed and accepted for publication. They are posted online prior to technical editing, formatting for publication and author proofing. The American Chemical Society provides “Just Accepted” as a free service to the research community to expedite the dissemination of scientific material as soon as possible after acceptance. “Just Accepted” manuscripts appear in full in PDF format accompanied by an HTML abstract. “Just Accepted” manuscripts have been fully peer reviewed, but should not be considered the official version of record. They are accessible to all readers and citable by the Digital Object Identifier (DOI®). “Just Accepted” is an optional service offered to authors. Therefore, the “Just Accepted” Web site may not include all articles that will be published in the journal. After a manuscript is technically edited and formatted, it will be removed from the “Just Accepted” Web site and published as an ASAP article. Note that technical editing may introduce minor changes to the manuscript text and/or graphics which could affect content, and all legal disclaimers and ethical guidelines that apply to the journal pertain. ACS cannot be held responsible for errors or consequences arising from the use of information contained in these “Just Accepted” manuscripts.



Instability of liquid Cu films on a SiO₂ substrate

Alejandro G. González,^{*,†,‡} Javier A. Diez,^{†,‡} Yueying Wu,[¶] Jason D. Fowlkes,[§]
Philip D. Rack,^{§,¶} and Lou Kondic^{||}

Instituto de Física Arroyo Seco, Universidad Nacional del Centro de la Provincia de Buenos Aires, Tandil, Argentina, CIFICEN-CONICET, Tandil, Argentina, Department of Materials Sciences and Engineering, University of Tennessee, Knoxville, TN, USA, Center for Nanophase Materials Sciences, Oak Ridge National Laboratory, TN, USA, and Department of Mathematical Sciences, New Jersey Institute of Technology, Newark, NJ, USA

E-mail: aggonzal@exa.unicen.edu.ar

Abstract

We study the instability of nanometric Cu thin films on a SiO₂ substrate. The metal is melted by means of laser pulses for some tens of nanoseconds, and during the liquid life time the free surface destabilizes, leading to the formation of holes at first and then in later stages of the instability to metal drops on the substrate. By analyzing the Fourier transforms of the SEM (scanning electron microscope) images obtained at different stages of the metal film evolution, we determine the emerging length scales at relevant stages of the instability development. The results are then discussed within the framework of a long-wave model. We find that the results may differ whether early or final stages of the instability are considered. Based on the interpretation of the experimental results, we discuss the influence of the parameters describing the interaction of the liquid metal with the solid substrate. By considering both the dependence of dominant length scales on the film thickness and

the measured contact angle, we isolate a model which predicts well the trends found in the experimental data.

Introduction

Instabilities of thin liquid films deposited on solid substrates have attracted a significant interest for a number of years. These instabilities are important in numerous applications, in particular in the fast growing field of nanofluidics. They lead to the formation of drops, which in the case of liquefied metals, solidify into particles, which find its relevance in the applications that range from plasmonics, to liquid crystal displays and solar cells;¹⁻³ for example, the size and distribution of metallic particles is known to be related to plasmon-coupling with incident energy, that has a huge potential of increasing the yield in solar cell devices.⁴ To make future progress of relevance to these and other applications, it is important to understand the basic mechanism driving the instabilities.

Stability of a thin film on nanoscale have been extensively studied in the case of polymer films, see, for instance, the recent review by Jacobs et al.⁵ However, metal films liquefied by laser irradiation, have been considered to a much smaller extent. Instabilities of Cu, Au, and Ni films were considered experimentally,⁶ and more recently both experimental and theoretical analyses of dewetting of Co, Ag, Fe, and Ni films have

*To whom correspondence should be addressed

[†]Instituto de Física Arroyo Seco, Universidad Nacional del Centro de la Provincia de Buenos Aires, Tandil, Argentina

[‡]CIFICEN-CONICET, Tandil, Argentina

[¶]Department of Materials Sciences and Engineering, University of Tennessee, Knoxville, TN, USA

[§]Center for Nanophase Materials Sciences, Oak Ridge National Laboratory, TN, USA

^{||}Department of Mathematical Sciences, New Jersey Institute of Technology, Newark, NJ, USA

1 been carried out.^{3,7-9} In our earlier works, we
2 have considered instabilities of other liquid metal
3 structures, such as polygons, lines, and rings.¹⁰⁻¹³
4 While these more complex geometries lead to ad-
5 ditional insight regarding the instability develop-
6 ment, it is important to analyze carefully the sim-
7 plest case (uniform films), since some of the the
8 basic mechanisms leading to instability in differ-
9 ent geometries are related. Therefore, a better un-
10 derstanding of uniform films should help us gain
11 better insight into the instability of more complex
12 structures.
13

14 For sufficiently thin metal films, of the thick-
15 nesses of few nanometers, there is a strong evi-
16 dence that the developing instability is of spinodal
17 type, i.e. it is caused by growth of surface per-
18 turbations due to destabilizing effect of liquefied
19 metal/substrate interaction forces.^{7,11} The instabil-
20 ity evolution proceeds typically by the formation
21 of holes in the liquid metal surface, and a net-
22 work of connected bridges. The rupture of these
23 bridges lead to a pattern of drops which solidify
24 to form isolated metal particles. The emerging
25 lengthscales – the distances between holes and/or
26 drops/particles – can then compared to theoretical
27 models expected to govern the evolution of the de-
28 scribed process. How to carry out this comparison
29 is not always clear - for example, one needs to de-
30 cide which stage of the instability development is
31 to be used. A most obvious question is whether the
32 distances between the holes that form in the initial
33 stages of the instability, or the distances between
34 the drops/particles that remain at the later times are
35 to be considered. To our knowledge, this issue has
36 not been analyzed carefully in the literature so far.
37 This is not surprising, since the evolution happens
38 on a very fast time scale and it is difficult to cap-
39 ture its properties. We will discuss this topic ex-
40 tensively in the present paper and study to which
41 degree the results are influenced by the temporal
42 evolution of the available data.
43

44 This work centers on experimental and theoret-
45 ical analysis of Cu films on SiO₂ substrate exposed
46 to laser irradiation. By considering the parts of
47 the experimental domain exposed to different ir-
48 radiance we are able to reach some understand-
49 ing regarding the time evolution of the instability,
50 and therefore distinguish between different stages
51 of its development. The Fourier spectrum of the

52 film thickness allows us to define in a precise man-
53 ner the emerging wavelengths and, in addition,
54 their time evolution. We should note here that the
55 data analysis that we carry out for the purpose of
56 quantifying the instability development is signifi-
57 cantly different from the one which was required
58 for polymer films, due to the difference in the type
59 of the available data. On one hand, the domain
60 sizes that can be used when liquid metals are con-
sidered is orders of magnitude larger than the typi-
cal instability wavelength, so that very good statis-
tics can be obtained. This is in contrast to poly-
mer films where domain size is typically a single
order of magnitude larger than the typical wave-
length, thus reducing the quality of the informa-
tion that can be reached based on Fourier spectra,
and requiring additional methods for data analy-
sis, e.g. based on Minkowski functionals.⁵ On the
other hand, the evolution in the case of metal films
happens much faster (on nanosecond time scales)
due to different material properties, and partially
for this reason precise information about temporal
evolution of instability is rarely available.

After carrying out Fourier spectra-based analysis
of the experimental data, we consider the applica-
tion of a long-wave (LW) model for the purpose
of studying the instability development. One has
to be careful regarding the choice of information
that is being used: in particular, we find that one
obtains different results when holes or drops are
considered. Note that previous works have usually
considered drops, since they are easier to study and
correspond to a fully developed final stage. How-
ever, there is no clear evidence whether the exper-
imental data obtained for drops could be reliably
related to existing linear theories or not. There-
fore, we discuss to which degree the LW model
within its linear regime can be used in conjunc-
tion with experimental data to extract the material
properties entering the governing model, such as
the Hamaker constant. Furthermore, we consider
different models describing liquid metal/solid sub-
strate interaction and discuss to how the choice of
a model influences the results.

Experiments

Copper thin films with thickness ranging from 4.8 nm to 15.5 nm were sputter deposited onto 100 nm SiO₂ coated silicon chips¹⁴ using radio frequency (RF) magnetron sources. The sputtering conditions are: 5 cm diameter sputter Cu targets and a RF power of 30 W (148 V self bias), 25 sccm Ar at 5 mTorr processing pressure. The Cu film thickness was measured via optical reflectometry (Filmetrics F20-UV thin-film analyzer).

The films were irradiated in air by either a single or multiple pulses using a normal incident laser beam (≈ 12 mm x 12 mm) that impinges at the center of the sample. The KrF laser has a wavelength of 248 nm and a Gaussian temporal profile whose width (full-width-at-half-maximum) is ≈ 18 ns. The laser energy density was chosen to be 140 mJ/cm² to ensure the films reach melting threshold based on the numerical simulation method used in our earlier work.¹³ The total fluency of energy received by the metal in a particular region during its irradiation determines the liquid lifetime. Since the laser energy has a Gaussian spatial profile, the decreasing energy density from the center to the edge of the thin films leads to different liquid lifetimes at different regions. This effect allows us to capture information of different stages of the evolution of the liquid film dewetting within a single pulse. Therefore, a region in the center of the pulse has longer liquid lifetime than the regions at the borders. The regions subject to lower fluency can be correlated to early dewetting stages, while those at higher fluency, as well as those irradiated with more pulses, have longer lifetimes and then correspond to later stages.

In contrast to the dewetting process of polymeric films where the dynamic evolution is readily accessible, since it takes place in time scales of the order of seconds, minutes, or even hours, the liquid metal thin films typically require nanoseconds and hence capturing experimentally different dewetting stages is a complex challenge. To this end, nano-second laser irradiation with a gradient energy distribution provides an effective way to freeze different stages corresponding to different liquid life times. Therefore, it is meaningful to explore the change in experimental length scales during morphology evolution considering differ-

ent regions, and determine which stage corresponds more closely to existing theoretical models and yields a better estimate of the Hamaker constant.

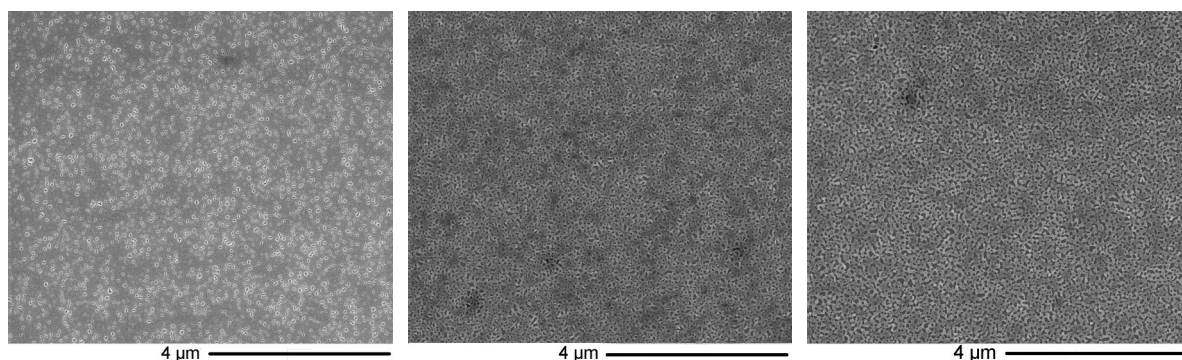
The morphologies of different stages of the evolution are captured by taking scanning electron microscopy (SEM) images after each pulse of the resolidified sample. In order to have a roughly consistent localization of the energy profile on the thin film after each laser pulse, we align the substrate at practically the same laser position. In this way, we are able to capture different dewetting stages as one moves from the center to the edge.

Figure 1 shows a typical case of the series of SEM pictures obtained in experiments for Cu films with a thickness of $h = 8.0$ nm on SiO₂. Figures 1a–d correspond to pictures taken at the border of the central region of the irradiated sample in a single laser pulse. In Fig. 1a, we observe a rather non uniform distribution of holes which becomes more uniform in Fig. 1b. As one considers a region closer to the center of the pulse, the holes become bigger and tend to coalesce, forming a net of rims. In Fig. 1d, the rims break up and retract leading to a new configuration which after a second pulse ends up in a distribution of drops (Fig. 1e). In summary, this type of analysis of the SEM's allows to correlate both the position of a picture with respect to the center of the pulse (and/or the number of pulses) with a time sequence that describes the evolution of the film instability.

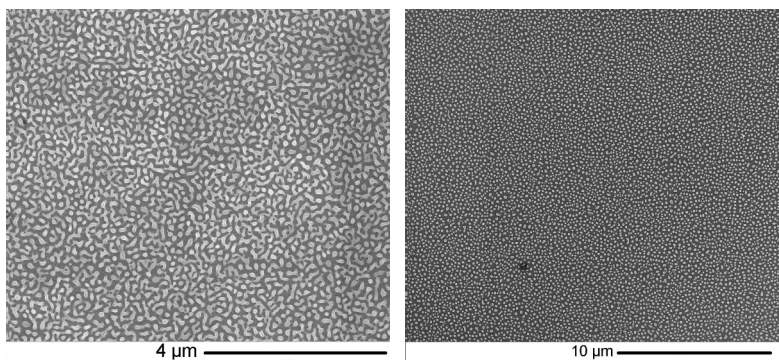
We have repeated the procedure in a series of 26 experiments with thickness varying from 4.8 nm to as high as 17 nm. We took an average of four pictures for each experiment corresponding to different stages. These images were used to compute the results given in the following section.

Measurement of contact angles

We now proceed to measure the static contact angles of the drops resulting after a large number of pulses. We have used two methods. The first one consists in applying a sufficient number of laser pulses to assure fully developed drops shape. The fluence is controlled and limited in order to minimize evaporation. Examples of these drops are shown in Fig. 2a, where the approximating spheres



26 (a) First stage: border, one pulse. (b) Second stage: outer intermedi- (c) Third stage: inner intermediate,
27 ate, one pulse. one pulse.



42 (d) Fourth stage: center, one pulse. (e) Last stage: center, two pulses.

43 Figure 1: SEM images of various regions of a 8.0nm thick Cu film on a SiO₂ substrate. The position
44 of each picture with respect to the center of the laser beam decreases from (a) to (d), and thus the corre-
45 sponding liquid lifetime increases. Picture (e) is also central as (d), but the film has been irradiated with
46 an extra pulse, and therefore it corresponds to the largest lifetime.
47
48
49
50
51
52
53
54
55
56
57
58
59
60

and the calculated contact angles are also shown. The distribution of these angles with respect to drop volumes is shown in Fig. 2b for drops obtained from films of different thicknesses. We observe a significant variation of θ for smaller drops ($V < 3 \times 10^{-3} \mu\text{m}^3$), while the mean value $\langle \theta \rangle$ vary from 69° to 80° . We note that a possible dependence of contact angle on the drop size is an interesting question, which we leave for future work. For the present purposes, the mean values are sufficient.

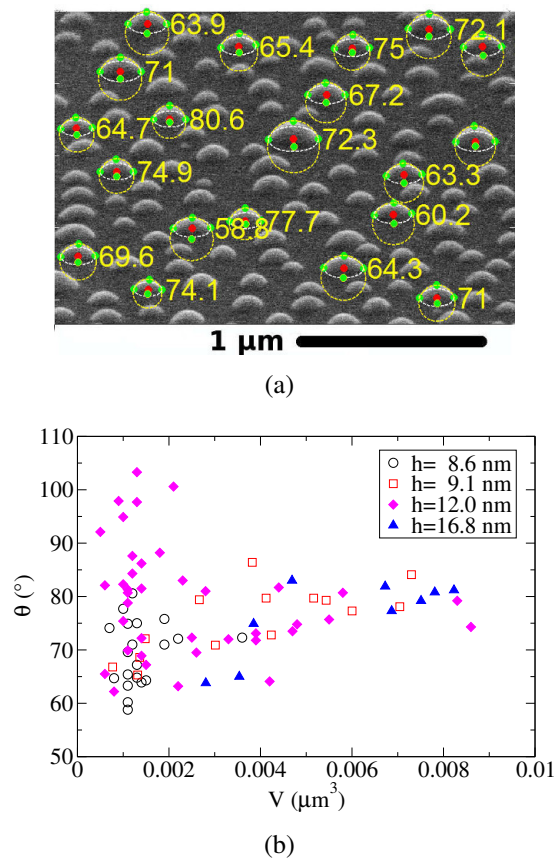


Figure 2: (a) Measurement of contact angles in a sample of solidified drops (particles) resulting from a film of thickness $h = 8.7$ nm. (b) Distribution of contact angles from films of different thickness, h , versus the drops volume.

A drawback of the method described above is that it is difficult to determine the points of contact at the base of a solidified drop, particularly the smaller ones. Therefore, we have also explored an alternative approach that enhances the contrast of the surface of a particle. To do so, we sputtered a thick layer of Ni (≈ 150 nm) on top of Cu drops, and then we milled them by means of a focused ion

beam (FIB). This milling process was done with an FEI Nova 600 dual beam scanning electron microscope (SEM) with a gallium ion source under an accelerating voltage of 30 KeV. The ion milling area was defined to show the whole drop cross section (≈ 800 nm \times 800 nm area in this case) and was carefully aligned through the center of the particle. After ion milling of each drop, cross section SEM images were taken to determine the contact angle as shown in Fig. 3. As a result, the average contact angle of a total of 15 drops is 65° with a standard deviation of 6.9° . This result is consistent with the one given above, suggesting that despite relatively large standard deviations, contact angle is a well defined quantity on the scales considered.

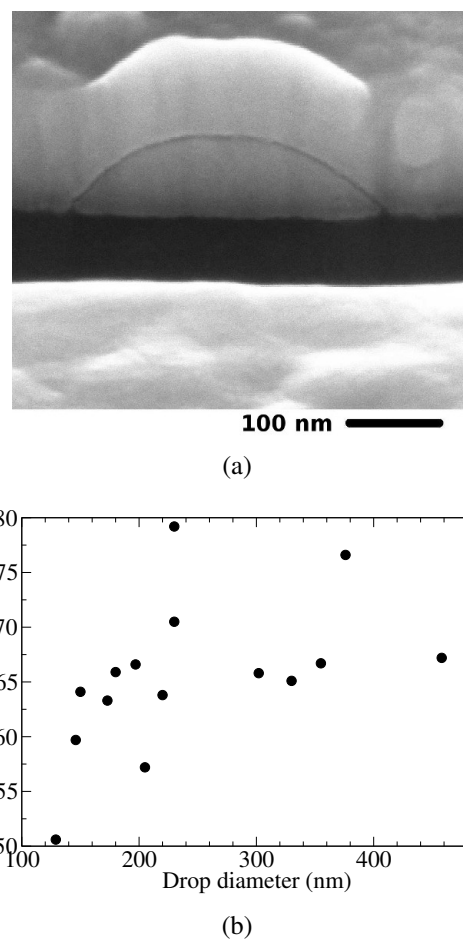


Figure 3: (a) Image of a solidified Cu drop covered with nickel and viewed with a 52° tilt. (b) Distribution of contact angles for different drops versus their projected diameters.

Evolution of the instability

In order to study the characteristic length scales of the patterns formed by the thin films instability, we have computed the fast Fourier transforms (FFT) of pictures corresponding to different stages of the evolution. For the reasons described in the next paragraph, we consider four sub-regions of 512×512 pixels at the corners of each picture (whose size is 2048×1764 pixels), and obtain the corresponding FFT's. First, we verify that there is no preferred direction in the film pattern. Figure 4 shows the density of the transform for a typical sub-region. The annular white zone confirms that the distribution of length scales is isotropic. We have verified that isotropic distribution holds for all considered experimental images.

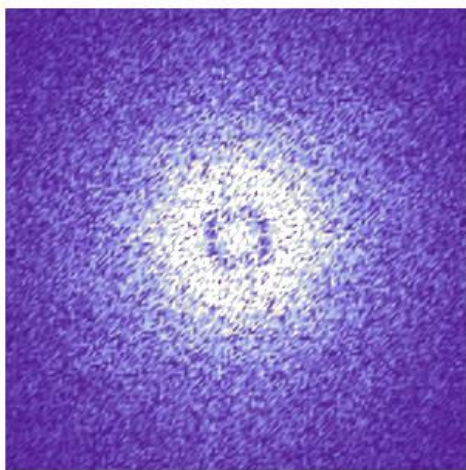


Figure 4: Density plot of the FFT of Fig. 1c.

Once confirmed that the FFT's are isotropic, we compute (for each of the four sub-regions) the radial spectral distribution of wavenumbers, k , by averaging the FFT's over all directions for annuli between k and $k + \delta k$. A good overlapping of the spectra for all four sub-regions guarantees that the whole picture corresponds to the same stage. Figure 5 shows that this is indeed the case, and therefore we conclude that each of the pictures shown in Fig. 1 corresponds to a fairly uniform laser irradiation, and have endured the same liquid lifetime. The peaks of the spectra can be correlated to typical lengths, $\ell = 2\pi/k$, which, depending on the stage under study, characterize the sizes and distances between holes or drops.

In order to describe the evolution of the film

instability, we must correlate the average radial spectra of a picture with a time sequence. For instance, in Fig. 1a there is a rather random pattern of holes, and so its average spectra has a weak and wide peak at $k_{max} \approx 100 \mu m^{-1}$ ($\ell_{max} \approx 63 nm$) as shown in Fig. 5a. This indicates that there is no clear dominant length in this very early stage. The apparent peak around $k = 0$ is an artifact of the method due to the finite size of the sample, and it is more pronounced in the early stages where there are rather extensive connected flat areas. Fig. 5b shows instead a spectra with a clear peak at $k_{max} \approx 63 \mu m^{-1}$ ($\ell_{max} \approx 100 nm$) in correspondence with the more uniform distribution of holes in Fig. 1b. This peak is due to the fact that there is a better defined spacing between holes. In the next stage, the holes are growing and coalescing thus leading to an increase in the characteristic spacing as seen in the peak at $k_{max} \approx 50 \mu m^{-1}$ ($\ell_{max} \approx 125 nm$) in Fig. 5c. At the fourth stage in Fig. 1d, the bridges and rims around the holes have broken up and have given place to a filament-like structure whose spectra is shown in Fig. 5d. This figure shows a narrower peak at a lower wavenumber $k_{max} \approx 38 \mu m^{-1}$ ($\ell_{max} \approx 166 nm$). As these elongated structures further contract and break up, a rather uniform distribution of drops shows up (see Fig. 1e). The spectrum shown in Fig. 5e has a peak at $k_{max} \approx 25 \mu m^{-1}$ ($\ell_{max} \approx 250 nm$), thus indicating the final drop spacing. The shape of these drops is very similar to spherical caps, and their average radius contributes to the formation of an incipient secondary peak in the spectra, as seen in Fig. 5e for $k \approx 69 \mu m^{-1}$ ($\ell \approx 90 nm$).

A typical evolution of these spacings is shown in Fig. 6a. Since the total liquid life time is not exactly known, we sort the lengths according to the stages, shown in Fig. 1, providing therefore a rough idea of the time evolution. The tendency of the pattern to increase its typical length scale is clearly visible. The error in the determination of the distances is calculated from the dispersion of the corresponding k 's obtained for each of the four sub-regions.

We find it useful to separate the evolution into four main stages:

1. a *preliminary early stage*, where no well-defined peak is observed in its spectrum;

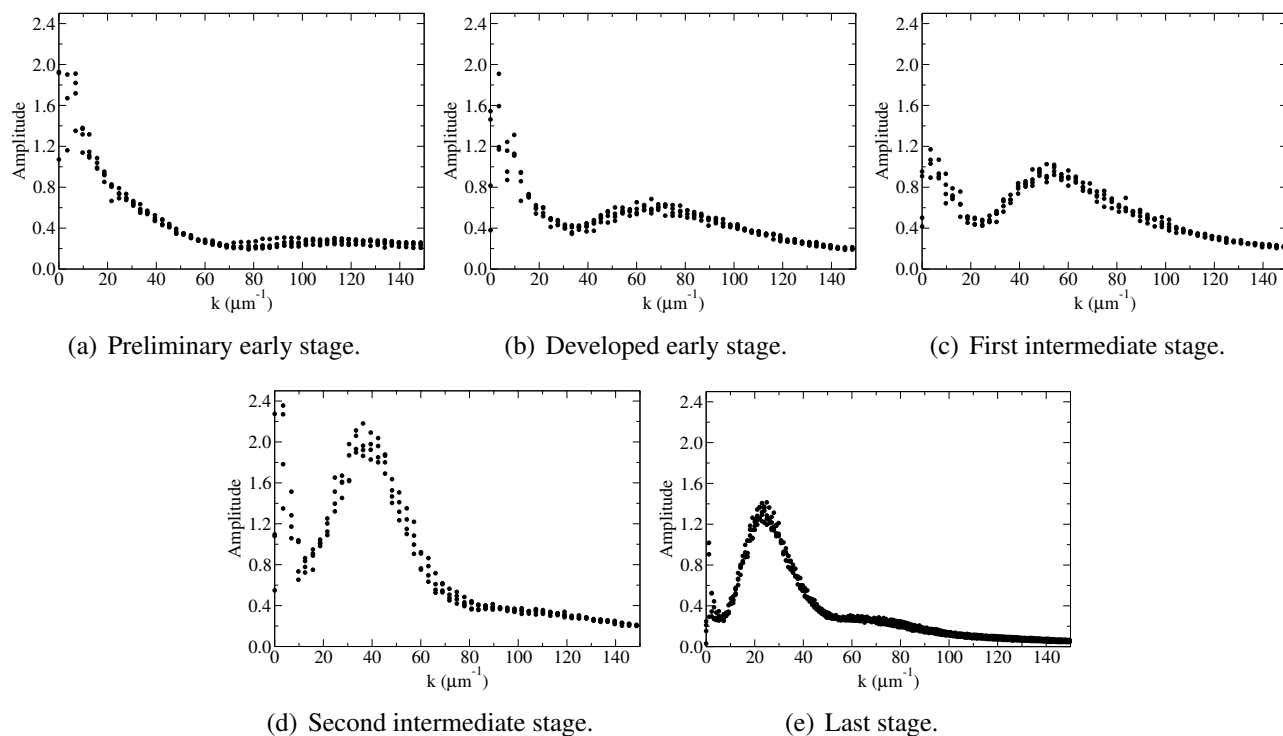


Figure 5: FFT spectra of the experimental images shown in Fig. 1. Each part of the figure shows four FFT spectra computed from four sub-domains of the experimental images. All the spectra are plotted with the same symbol. The overlap shows that the patterns in each experimental figure belong to the same stage of the evolution. The exposure time increases from (a) to (e).

2. a *developed early stage*, where the holes distribution is characterized by a clear peak;
3. a series of *intermediate stages*, where bridge breakups and coalescence are produced; and
4. a *final stage*, where drops are clearly visible and characterized by a narrow peak in the spectrum.

The first length scale, ℓ_{max} , which appears in the evolution corresponds to the *developed early stage*, and it characterizes the distance between the centers of the holes formed in the film. We denote such length as ℓ_{holes} . Similarly, when the instability saturates to a final pattern of drops, ℓ_{max} corresponds to the average distance between drop centers, which we call ℓ_{drops} (see Fig. 6b).

While analyzing the information from more than 450 spectra, we have found consistently a monotonic increase of ℓ_{max} as we progress from the early second stage to the advanced fourth one above. Therefore, by studying the early second stage (when the thin film linear instability is fully

developed, but not affected by nonlinear effects or other types of instability) and the fourth stage (when the drops are completely formed), we cover the full range of emerging length scales. Furthermore, intermediate stages are conceptually complicated to consider since they involve coupling of linear and nonlinear effects. For these reasons, we concentrate on the developed early stage and on the final stage in what follows.

Modeling of the instability

The typical length scales obtained from the spectra discussed in the previous section are analyzed within the framework of the linear thin film instability under the LW model. In this approach, it is assumed that the flow is driven by both surface tension and van der Waals forces. The latter are described by the so-called disjoining pressure, Π , whose dependence on thickness h involves the competition between long- and short-range forces.¹⁵ While the exact function form of Π is not known, in particular for liquid metals^{11,16}

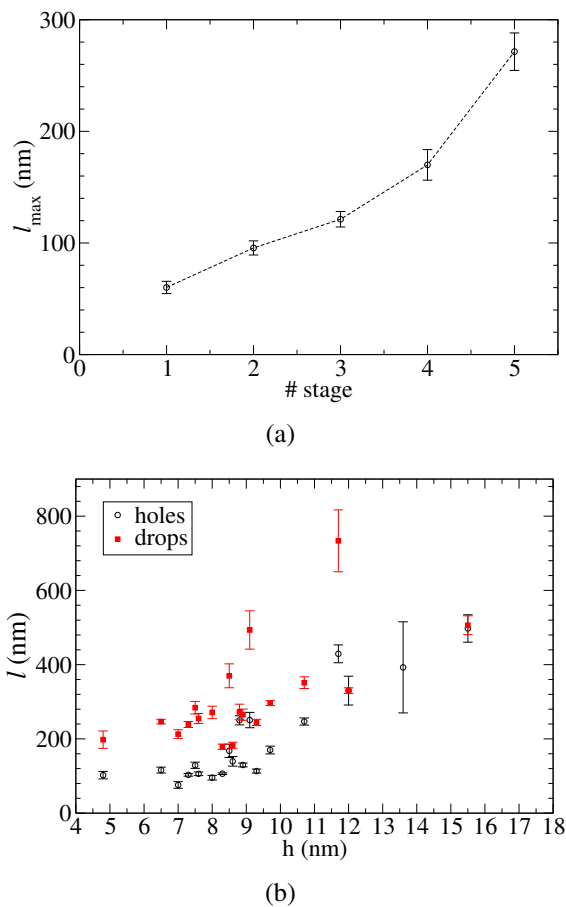


Figure 6: (a) Evolution of the characteristic spacing of the patterns, l_{max} for the experimental images shown in Fig. 1. The horizontal axis indicates the numbering of the stage. (b) Average distance between holes (l_{holes}) at the *developed early stage* and drops (l_{drops}) at the *final stage* for different film thickness, h .

(see these references for further discussion), a commonly used expression is^{17–19}

$$\Pi(h) = \kappa \left[\left(\frac{h_*}{h} \right)^n - \left(\frac{h_*}{h} \right)^m \right], \quad (1)$$

where h is the fluid thickness, $n > m$ are positive exponents, and h_* is the equilibrium thickness where repulsive and attractive forces balance. Within the present context, the second term includes the electronic component.²⁰ The pressure scale, κ , is related to the Hamaker constant, A , as

$$A = 6\pi\kappa h_*^3, \quad (2)$$

Only a small subset of exponents (n, m) has been considered in previous works. It is difficult to ob-

tain them from very first principles, except using additional simplifying assumptions that cannot be always taken for granted in liquid metal films subject to laser irradiation. Typical examples found in the literature²¹ considering polymeric films are: (9, 3), (4, 3) and (3, 2). For liquid metals, some of these exponents have been used, and both simplified versions with attractive forces only,^{3,7,8} and more complex models with additional exponential term²² have been used.

Since it is unclear from the literature which exponents should be used, in the present work we will explore whether a simple model, specified by Eq. (1), with (commonly used) sets of exponents provides consistent results, and/or whether one could identify the pair which provides a good agreement with the experimental results for Cu, while remembering that the functional form specified by Eq. (1) is an approximation itself. Another approximation - the use of the LW model for a problem where equilibrium contact angles are large - should be recalled as well. We expect that this approach is applicable in particular when considering initial stages of instability (leading to hole formation) since during most of the instability development the slopes of the film surface are not too large.

Using this disjoining pressure within the LW model, the wavelength of the mode of maximum growth rate obtained from the linear stability analysis (LSA) is given by²³

$$\lambda_m = 2\pi / \sqrt{\frac{A}{12\pi\gamma h h_*^3} \left[m \left(\frac{h_*}{h} \right)^m - n \left(\frac{h_*}{h} \right)^n \right]}, \quad (3)$$

where γ is the liquid surface tension. Since this formula refers to the linear regime, it is appropriate to assume that λ_m should be related to l_{holes} , although it is frequently found in the literature that it is related to l_{drops} (as well). We also consider this possibility and discuss its implications in an appropriate section below. Here, we proceed to discuss the basic framework which can be used to compare the experimental results to the predictions of the model leading to Eq. (3). We note that typical values of h_* are estimated in the theories that describe the intermolecular interactions, such as those using Lennard-Jones potentials, and they

suggest h_* of the order of a few Å.²⁴

To proceed, we first study in some detail the behavior of Eq. (3) with respect to the exponents (n, m) . It is convenient to rewrite this equation as

$$\lambda_m = \sqrt{\frac{48\pi^2\gamma}{mA} h^{m+1} h_*^{3-m} \left[1 - \frac{n}{m} \left(\frac{h_*}{h} \right)^{n-m} \right]^{-1}}. \quad (4)$$

Since $h_* \ll h$ for the considered experiments, the square bracket is approximately equal to unity, and consequently λ_m becomes independent of the exponent n , which accounts for the repulsive force term in Eq. (1). Moreover, for $m = 3$, the dependence on h_* also disappears, and we have

$$\lambda_m = \sqrt{\frac{16\pi^3\gamma}{A} h^2}, \quad \text{for } m = 3, \quad (5)$$

which is an expression frequently used in the literature,^{7,8,25} albeit for different metals. For $m \neq 3$, the functional dependence of λ_m on both h and h_* is modified. In particular, for $m = 2$ as, for instance, in the commonly used pair (3,2), we have

$$\lambda_m = \sqrt{\frac{24\pi^3\gamma}{A} h^{3/2} h_*^{1/2}}, \quad \text{for } m = 2. \quad (6)$$

Regarding the time scales involved in the problem, the LSA gives

$$\tau = \frac{3\mu}{16\gamma\pi^4} \frac{\lambda_m^4}{h^3}, \quad (7)$$

where μ is the fluid viscosity. Thus, we have

$$\tau = \frac{48\pi^2\gamma\mu}{A^2} h^5, \quad \text{for } m = 3, \quad (8)$$

and

$$\tau = \frac{108\pi^2\gamma\mu}{A^2} h_*^2 h^3, \quad \text{for } m = 2. \quad (9)$$

Note that $m = 2$ case retains the dependence on h_* unlike the $m = 3$ case, and this implies that the instability develops much faster for the pair (3,2) than for pairs such as (9,3) and (4,3), since $h_* \ll h$.

The static contact angle, θ , of the drops resulting from the instability process can be related to the parameters κ and h_* of the disjoining pressure by

23

$$\kappa = \frac{\gamma}{2Mh_*} \tan^2 \theta, \quad (10)$$

where $M = (n - m)/((m - 1)(n - 1))$. Note that here we are assuming the dependence on θ in the form of $(\tan^2 \theta)/2$ instead of $(1 - \cos \theta)$, since the former dependence^{23,26} results from the linearized form of the free surface curvature,²⁷ consistently with the hypothesis of small slope in the LW model, while the latter is derived from the complete (nonlinear) form. By using Eq. (2), we can now express θ in terms of the Hamaker constant, A , and the equilibrium thickness, h_* ,

$$\tan \theta = \sqrt{\frac{MA}{3\pi\gamma h_*^2}}. \quad (11)$$

In the next two sections we proceed to discuss the utility of the outlined expressions for λ_m and θ for the purpose of explaining the experimental results.

Analysis based on the distances between holes

The early stages of the thin film instability, for which the LSA is appropriate, yields as immediate consequence to the formation of holes. Since during a considerable part of this hole formation process the slopes of the film surface are not large, the LW model should accurately describe the dynamics. The process leading to drop formation is much more complex. Therefore, we consider the distance between holes first.

Since one expects that ℓ_{holes} is basically given by λ_m as predicted by the LSA within the LW model, we attempt to fit the experimental values of ℓ_{holes} with Eq. (3). To do so, we start by choosing two pairs of exponents (9,3) and (4,3), and a value of $h_* = 0.1\text{nm}$ that is consistent with the underlying theories. Figure 7 shows that the fittings with both pairs are very similar, which according to Eq (2) yield $A = 1.36 \times 10^{-16}$ J. This value is significantly larger than the reported by Eichenlaub et al.,^{28,29} which vary between a theoretically calculated value of $A_{calc} = 1.67 \times 10^{-19}$ J and an experimentally measured one of $A_{exp} = 1.42 \times 10^{-19}$ J. One may wonder whether the assumed value of h_*

is too small; however, even for h_* as large as 2nm or so, too high values of A are obtained. Even if Eichenlaub's deductions are disregarded, the values of the Hamaker constant obtained using the pairs of exponents (9,3) and (4,3) are too large to be acceptable in comparison to other results reported in the literature.^{3,9,30} Note also h_* of the order of a few nanometers is inconsistent with the underlying molecular models. These results suggest that $m = 3$ for any usual $n > m$ does not lead to acceptable values of A for the considered experimental case of Cu on SiO₂ substrate; it is possible that different metals and/or different substrates may lead to a different conclusion.

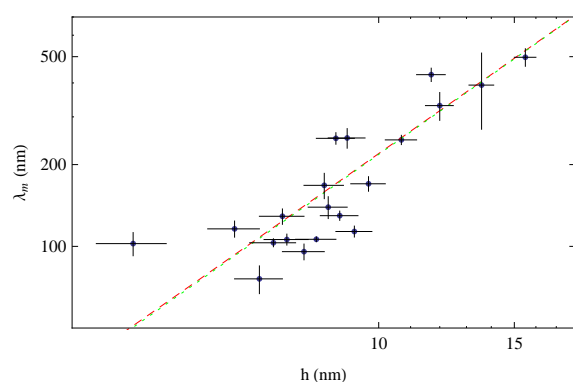


Figure 7: Fitting of ℓ_{holes} (symbols) with λ_m for $h_* = 0.1\text{nm}$. Both exponents (9,3) (dotted line) and (4,3) (dashed line) yield $A = 1.36 \times 10^{-16}$ J.

Next, we consider $m = 2$ and, in particular, the pair (3,2) which has also been suggested in the literature. Figure 8 shows the results for $h_* = 0.1\text{nm}$ (solid line) which leads to $A = 2.58 \times 10^{-18}$ J. This value, although still larger than those reported by Eichenlaub et al.,^{28,29} is two orders of magnitude smaller than the one obtained for $m = 3$, and furthermore it is comparable to other results reported in the literature.^{3,9,30} Figure 8 also shows that, as expected, the exponents (9,3) and (4,3) for this value of A cannot be used to fit the experimental data (dashed and dotted lines in Fig. 8).

We note that the fitting of ℓ_{holes} versus h with Eq. (6) for λ_m is obtained for a given value of the ratio A/h_* , provided $h_* \ll h$. In fact, we find an approximate linear relationship between the values of A obtained by varying h_* and using the full expression for λ_m , Eq. (4) (symbols in Fig. 9a). The small departure with respect to the average straight

line $A = 2.89 \times 10^{-17}h_*$ J, with h_* in nm, is due the additional term with $n = 3$. This result implies that in order to obtain A as small as 10^{-19} J, one needs to consider $h_* \approx 0.01\text{nm}$, which is unacceptably small from the physical point of view.

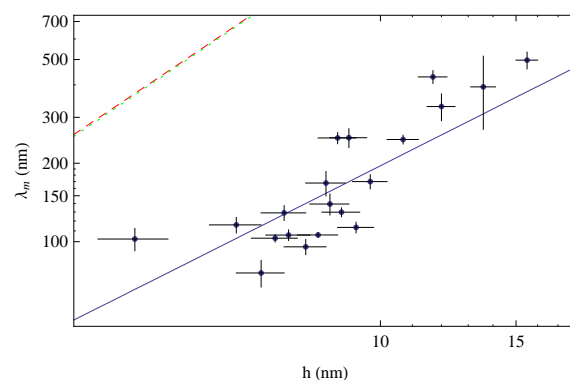


Figure 8: Fitting of ℓ_{holes} (symbols) with λ_m for $h_* = 0.1\text{nm}$. The exponents (3,2) (solid line) yield $A = 2.58 \times 10^{-18}$ J, while (4,3) (dashed line) and (9,3) (dotted line) are unable to fit the data.

Finally, by using a linear approximation for the relation between A and h_* for (3,2) in Eq. (11), we can relate θ with h_* as shown in Fig. 9b. For $h_* = 0.1\text{nm}$, Eq. (11) yields $\theta = 72.8^\circ$, which is in reasonable agreement with the measured contact angles (see Figures 2 and 3). This can be interpreted as a further confirmation of the selection of exponents (3,2), since the theory gives theoretical angles that are in correspondence with independently measured ones.

We note that several factors may contribute to yield a Hamaker constant larger than that reported by Eichenlaub et al.²⁹ The studies based on Lifshitz theory,²⁴ have demonstrated that Van der Waals or Casimir forces can be modified due to a change of the optical properties of the materials.³¹⁻³⁸ This change can be produced by the generation of extra free electrons due to the laser irradiation, which may take place in our case in both metal and Si under the 100nm SiO₂ layer. For instance, under an irradiation of a 1.7ns (full width half maximum) laser with an effective energy of 30 μJ and a photon energy of 3.68eV, Inui³⁷ reported an increase of Casimir force between two 100nm thick Si plates with a separation of 1 μm of about 1.5 times the force without laser irradiation. In our case, the free carrier generation

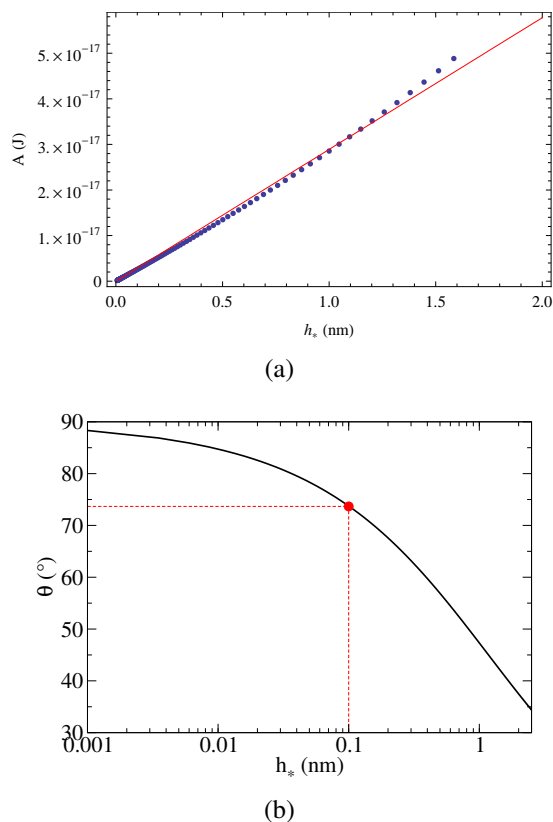


Figure 9: (a) Hamaker constant, A , versus h_* from the fitting of ℓ_{holes} with λ_m . The solid line shows an average linear relationship. (b) Contact angle, θ , versus h_* for (3,2). The symbol on the curve corresponds to the predicted contact angle for $h_* = 0.1 \text{ nm}$ ($\theta = 72.8^\circ$).

rate under the laser pulse energy of 0.14 J/cm^2 can reach above $10^{16} - 10^{17} \text{ cm}^{-3}$ per nanosecond, and hence a modified dielectric constant is expected. As for the metal film, modified dielectric constant and nonlinear optical response under ultrafast laser irradiation have been widely explored.^{39–41} Bigot et al.⁴² used an 80fs pump laser with a maximum pump energy density of 0.5 mJ/cm^2 to investigate the effect of interband and intraband transition on optical properties of Cu nanoparticles. With a modified energy status distribution due to an increase of electron temperature³⁹ and enhancement of Fermi energy as a result of interband transitions, as well as a different inverse collision time of the collective mode, it is showed that the corresponding dielectric constant can be modified by the laser excitation. Comparing the laser energy density used by Bigot et al. ($6 \times 10^{-6} \text{ J/fs cm}^2$) to the laser energy density applied in our experi-

ment ($\approx 8 \times 10^{-6} \text{ J/fs cm}^2$), a similar phenomenon may take place in our Cu film while the laser duration is much longer than a femtosecond laser. Besides the laser effect, an increased temperature that may smear the electronic distribution around the Fermi energy can also modify the liquid metal optical constant. This brief discussion provides only some of the possibilities that may lead to an increase of the actual Hamaker constant. Further work is needed to understand how relevant any of these effects actually is.

Analysis based on the distances between drops

The distance between drops, ℓ_{drops} , has been also considered in determining the characteristic length scale of the instability, despite the fact that drops are the outcome of complex dynamics which is not necessarily well described (if at all) by the linear stability analysis. Still, we consider drops as well in order to illustrate the differences in the results when considering drops versus holes. Figure 10 shows the distance between the drops, and corresponding fits obtained using Eq. (3) for $h_* = 0.1 \text{ nm}$, and the same pairs of exponents as in previous section. Due to the larger dispersion of the experimental results, the linear regression in the log-log plot in the figure is not so good as for ℓ_{holes} ; for instance, the standard deviation of the data with respect to the fit is now almost twice as large. Nevertheless, the pair (3,2) still yields a reasonable fit for ℓ_{drops} , while pairs such as (9,3) and (4,3) lead to fitting lines which do not describe the experimental results well. The (3,2) pair leads to the best fit for a Hamaker constant $A = 7.18 \times 10^{-19} \text{ J}$, which is smaller than the one obtained with ℓ_{holes} , and it is coincidentally closer to the reported values.²⁸ However, following a similar procedure to the one described in the previous section to calculate the contact angle, we find $\theta = 59.7^\circ$, which is out of the range of the measured angles (see Fig. 2b and Fig. 3b). As discussed previously, this finding is not surprising due to the complexity of nonlinear effects which are responsible for the drop formation.

The failure to get a good fit for drops, and the reasonable results for holes, is not so surprising if

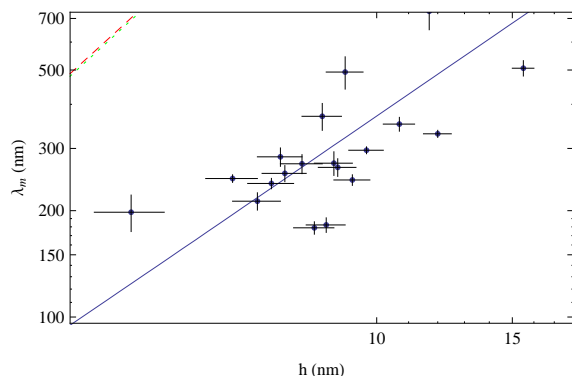


Figure 10: Fitting of ℓ_{drops} (symbols) with λ_m for $h_* = 0.1\text{nm}$. The exponents (3,2) (solid line) yield $A = 2.58 \times 10^{-18}\text{ J}$, while (4,3) (dashed line) and (9,3) (dotted line) do not provide good fits for this value of A .

one takes into account that the considered model is based on the linear stability analysis, and therefore small perturbations from a base state (flat film). Furthermore, one also cannot expect a good agreement with the theory by considering intermediate stages of instability, since during these stages nonlinear effects already become dominant. The intermediate stages can provide interesting information about growth rates, mixing of instabilities or evolution to a nonlinear regime, but these studies will require further extensive analysis that is out of the scope of the present work.

Conclusions

In this paper, we have considered the evolution of the instability of Cu films on SiO_2 substrates, where the metal is liquefied by exposure to laser irradiation. One distinguishing feature of this study is that, by analyzing regions of the film exposed to different levels of irradiation, we are able to define several stages of the instability development. When considering initial stages, we find a clear signature of the spinodal type of instability manifesting itself in a well defined peak in the Fourier spectrum, and thus suggesting the existence of a length scale that characterizes the emerging features. The experimental results are then analyzed using a long-wave (LW) model. The wavelength of maximum growth rate as given by the linear stability analysis performed within this model al-

lows to extract the values of the Hamaker constant describing the liquid metal/solid substrate interaction. The values thus obtained are found to be larger than expected based on the (limited) available literature, but consistent with other works considering similar systems. We find that the functional form of the disjoining pressure model describing liquid/solid interaction has a strong influence on the comparison between the experiment and the theory; only one of the usual exponent pairs defining the disjoining pressure can provide a reasonable fit to the experimental results. Furthermore, significantly different results are found when the model is applied to the drops/particles (which are formed in the last stages of the instability development and do not change their shape with additional laser pulses) instead of holes that form during early stages. This suggests that much care is required when applying the tools of LW (or any other) theory for the purpose of understanding the experimental data: the conclusions may be sensitive to the properties of the considered model, as well as to the choice of the time at which the experimental data are extracted. For example, the standard results regarding scaling of the emerging length and time scales with the film thickness, h , do depend on the parameters entering the model. For the present study of Cu films on SiO_2 substrates we find that the exponent pair (3,2) provides a good agreement for the scaling of the wavelength, λ , with h , ($\lambda \sim h^{3/2}$), while the other pairs of exponents, leading to $\lambda \sim h^2$, do not provide accurate description of the experimental data, at least for the system considered here.

The results given in this paper show that linear stability analysis of the underlying LW model, when used carefully, can be utilized for developing an accurate description of the experimental data. We expect that these results will bring us a step closer in developing better understanding of the instability evolution in other, more complex liquid metal geometries. This will be a subject of our future work.

Acknowledgement J.D.F. and Y.W. acknowledge support from the U.S.Department of Energy, Basic Energy Sciences, Materials Sciences and Engineering Division. P.D.R. and L.K. acknowledge partial support by the NSF Grant No.

1 CBET 1235710. A portion of this work was con-
2 ducted at the Center for Nanophase Materials Sci-
3 ences, which is sponsored at Oak Ridge National
4 Laboratory by the Office of Basic Energy Sci-
5 ences, U.S. Department of Energy. A.G.G. and
6 J.A.D. acknowledge support from Consejo Na-
7 cional de Investigaciones Científicas y Técnicas
8 de la República Argentina (CONICET, Argentina)
9 with grant PIP 844/2011 and visits to ORNL with
10 a joint CONICET-NSF international cooperation
11 project.
12
13

14 References

- 15
16
17 (1) Maier, S. A.; Kik, P. G.; Atwater, H. A.;
18 Meltzer, S.; Harel, E.; Koel, B. E.; Re-
19 quicha, A. A. Local detection of electromag-
20 netic energy transport below the diffraction
21 limit in metal nanoparticle plasmon waveg-
22 uide. *Nat. Mater.* **2003**, *2*, 229–232.
23
24 (2) Sun, S.; Murray, C.; Weller, D.; Folks, L.;
25 Moser, A. Monodisperse FePt nanoparticles
26 and ferromagnetic FePt nanocrystal superlat-
27 tices. *Science* **2000**, *287*, 1989–1992.
28
29 (3) Krishna, H.; Shirato, N.; Favazza, C.; Kalya-
30 naraman, R. Energy driven self-organization
31 in nanoscale metallic liquid films. *Phys.*
32 *Chem. Chem. Phys.* **2009**, *11*, 8136–8143.
33
34 (4) Maier, S. *Plasmonics: Fundamentals and*
35 *Applications*; Springer-Verlag: New York,
36 2007.
37
38 (5) Jacobs, K.; Herminghaus, S.; Seemann, R. In
39 *Thin liquid films*; Tsui, O., Russel, T., Eds.;
40 World Scientific, 2008; p 243.
41
42 (6) Herminghaus, S.; Jacobs, K.; Mecke, K.;
43 Bischof, J.; Fery, A.; Ibn-Elhaj, M.;
44 Schlagowski, S. Spinodal Dewetting in Liq-
45 uid Crystal and Liquid Metal Films. *Science*
46 **1998**, *282*, 916–919.
47
48 (7) Favazza, C.; Kalyanaraman, R.; Sureshku-
49 mar, R. Robust nanopatterning by laser-
50 induced dewetting of metal nanofilms. *Nan-*
51 *otechnology* **2006**, *17*, 4229–4234.
52
53 (8) Trice, J.; Thomas, D.; Favazza, C.; Sureshku-
54 mar, R.; Kalyanaraman, R. *Phys. Rev. Lett.*
55 **2008**, *101*, 017802.
56 (9) McKeown, J. T.; Roberts, N. A.;
57 Fowlkes, J. D.; Wu, Y.; LaGrange, T.;
58 Reed, B. W.; Campbell, G. H.; Rack, P. D.
59 Real-Time Observation of Nanosecond
60 Liquid-Phase Assembly of Nickel Nanopar-
 ticles via Pulsed-Laser Heating. *Langmuir*
 2012, *28*, 17168–17175.
 (10) Kondic, L.; Diez, J.; Rack, P.; Guan, Y.;
 Fowlkes, J. Nanoparticle assembly via the
 dewetting of patterned thin metal lines: Un-
 derstanding the instability mechanism. *Phys.*
 Rev. E **2009**, *79*, 026302.
 (11) Wu, Y.; Fowlkes, J. D.; Rack, P. D.;
 Diez, J. A.; Kondic, L. On the breakup of pat-
 terned nanoscale copper rings into droplets
 via pulsed-laser-induced dewetting: com-
 peting liquid-phase instability and transport
 mechanisms. *Langmuir* **2010**, *26*, 11972–
 11979.
 (12) Wu, Y.; Fowlkes, J. D.; Roberts, N. A.;
 Diez, J. A.; Kondic, L.; González, A. G.;
 Rack, P. D. Competing liquid phase insta-
 bilities during pulsed laser induced self-
 assembly of copper rings into ordered
 nanoparticle arrays on SiO₂. *Langmuir* **2011**,
 27, 13314.
 (13) Fowlkes, J. D.; Kondic, L.; Diez, J.;
 Rack, P. D. Self-Assembly versus Directed
 Assembly of Nanoparticles via Pulsed Laser
 Induced Dewetting of Patterned Metal Films.
 Nano Lett. **2011**, *11*, 2478–2485.
 (14) Klein, K.; Melechko, A.; Rack, P.;
 Fowlkes, J.; Meyer, H.; Simpson, M.
 Cu–Ni composition gradient for the cat-
 alytic synthesis of vertically aligned carbon
 nanofibers. *Carbon* **2005**, *43*, 1857–1863.
 (15) Seemann, R.; Herminghaus, S.; Jacobs, K.
 Dewetting patterns and molecular forces: a
 reconciliation. *Phys. Rev. Lett.* **2001**, *86*,
 5534.

- 1
2
3
4
5
6
7
8
9
10
11
12
13
14
15
16
17
18
19
20
21
22
23
24
25
26
27
28
29
30
31
32
33
34
35
36
37
38
39
40
41
42
43
44
45
46
47
48
49
50
51
52
53
54
55
56
57
58
59
60
- (16) Ajaev, V.; Willis, D. Thermocapillary flow and rupture in films of molten metal on a substrate. *Phys. Fluids* **2003**, *15*, 3144.
- (17) Mitlin, V. S. On dewetting conditions. *Colloids and Surfaces* **1994**, *89*, 97–101.
- (18) Schwartz, L. W. Hysteretic Effects in Droplet motion on Heterogenous Substrates: Direct Numerical Simulation. *Langmuir* **1998**, *14*, 3440.
- (19) Mitlin, V. Dewetting revisited: New asymptotics of the film stability diagram and the metastable regime of nucleation and growth of dry zones. *J. Colloid Interface Sci.* **2000**, *227*, 371–379.
- (20) Derjaguin, B.; Leonov, L.; Roldughin, V. Disjoining pressure in liquid metallic films. *J. Colloid Interface Sci.* **1985**, *108*, 207–214.
- (21) Craster, R. V.; Matar, O. K. Dynamics and stability of thin liquid films. *Rev. Mod. Phys.* **2009**, *81*, 1131–1198.
- (22) Krishna, H.; Sachan, R.; Strader, J.; Favazza, C.; Khenner, M.; Kalyanaraman, R. Thickness-dependent spontaneous dewetting morphology of ultrathin Ag films. *Nanotechnology* **2010**, *21*, 155601.
- (23) Diez, J.; Kondic, L. On the breakup of fluid films of finite and infinite extent. *Phys. Fluids* **2007**, *19*, 072107.
- (24) Israelachvili, J. N. *Intermolecular and surface forces*; Academic Press: New York, 1992; second edition.
- (25) Trice, J.; Thomas, D.; Favazza, C.; Suresh Kumar, R.; Kalyanaraman, R. *Phys. Rev. B* **2007**, *75*, 235439.
- (26) Schwartz, L.; Eley, R. Simulation of Droplet Motion on Low-Energy and Heterogeneous Surfaces. *J. Colloid Interface Sci.* **1998**, *202*, 173.
- (27) Münch, A.; Wagner, B. Contact-line instability of dewetting thin films. *Physica D* **2005**, *209*, 178–190.
- (28) Butt, H.-J.; Kappl, M. *Surface and Interfacial Forces*; Wiley-VCH Verlag: Weinheim, 2010.
- (29) Eichenlaub, S.; Chan, C.; Beaudoin, S. P. Hamaker Constants in Integrated Circuit Metalization. *J. Colloid Interface Sci.* **2002**, *248*, 389–397.
- (30) Shirato, N.; Krishna, H.; Kalyanaraman, R. Thermodynamic modeling for the dewetting instability in ultra thin films. *J. Appl. Phys.* **2010**, *108*, 024313.
- (31) Chen, F.; Klimchitskaya, G. L.; Mostepanenko, V. M.; Mohideen, U. Control of the Casimir force by the modification of dielectric properties with light. *Phys. Rev. B* **2007**, *76*, 035338.
- (32) Chan, H. B.; Bao, Y.; Zou, J.; Cirelli, R. A.; Klemens, F.; Mansfield, W. M.; Pai, C. S. Measurement of the Casimir Force between a Gold Sphere and a Silicon Surface with Nanoscale Trench Arrays. *Phys. Rev. Lett.* **2008**, *101*, 030401.
- (33) Bao, Y.; Guérout, R.; Lussange, J.; Lambrecht, A.; Cirelli, R. A.; Klemens, F.; Mansfield, W. M.; Pai, C. S.; Chan, H. B. Casimir Force on a Surface with Shallow Nanoscale Corrugations: Geometry and Finite Conductivity Effects. *Phys. Rev. Lett.* **2010**, *105*, 250402.
- (34) Klimchitskaya, G. L.; Mohideen, U.; Mostepanenko, V. M. The Casimir force between real materials: Experiment and theory. *Rev. Mod. Phys.* **2009**, *81*, 1827–1885.
- (35) Arnold, W.; Hunklinger, S.; Dransfeld, K. Influence of optical absorption on the Van der Waals interaction between solids. *Phys. Rev. B* **1979**, *19*, 6049–6056.
- (36) Klimchitskaya, G. L. Normal and lateral Casimir force: Advances and prospects. *J. Phys.: Conf. Ser.* **2010**, *258*, 012001.
- (37) Inui, N. Change in the Casimir force between semiconductive bodies by irradiation. *J. Phys.: Conf. Ser.* **2007**, *89*, 012018.

- 1 (38) Vogel, T.; Dodel, G.; Holzhauer, E.; Salz-
2 mann, H.; Theurer, A. High-speed switch-
3 ing of far-infrared radiation by photoioniza-
4 tion in a semiconductor. *Appl. Opt.* **1992**, *31*,
5 329–337.
6
- 7 (39) Shirato, N.; Krishna, H.; Kalyanaraman, R.
8 Ultrafast nonlinear mirrors with broad spec-
9 tral and angular bandwidths in the visible
10 spectral range. *Opt. Express* **2013**, *21*, 3573–
11 3581.
12
- 13 (40) Hopkins, P. E. Influence of inter- and intra-
14 band transitions to electron temperature de-
15 cay in noble metals after short pulsed laser
16 heating. *J. Heat Transfer* **2010**, *132*, 122402.
17
- 18 (41) Voisin, C.; Del Fatti, N.; Christofilos, D.;
19 Vallée, F. Ultrafast Electron Dynamics and
20 Optical Nonlinearities in Metal Nanoparti-
21 cles. *J. Phys. Chem. B* **2001**, *105*, 2264–2280
22
23 Phys. Rev. Lett. 1995, *75*, 4702.
24
- 25 (42) Bigot, J. Y.; Merle, J. Y.; Cregut, O.;
26 Daunois, A. Electron Dynamics in Copper
27 Metallic Nanoparticles Probed with Fem-
28 tosecond Optical Pulses. *Phys. Rev. Lett.*
29 **1995**, *75*, 4702–4705.
30
31
32
33
34
35
36
37
38
39
40
41
42
43
44
45
46
47
48
49
50
51
52
53
54
55
56
57
58
59
60

TOC Graphic

